When X-Rays Do Not Work. Characterizing the Internal Structure of Fossil Hominid Dentognathic Remains Using High-Resolution Neutron Microtomographic Imaging

Clément Zanolli, Burkhard Schillinger, Ottmar Kullmer, Friedemann Schrenk, Jay Kelley, Gertrud E Rössner, Roberto Macchiarelli

▶ **To cite this version:**

Clément Zanolli, Burkhard Schillinger, Ottmar Kullmer, Friedemann Schrenk, Jay Kelley, et al.. When X-Rays Do Not Work. Characterizing the Internal Structure of Fossil Hominid Dentognathic Remains Using High-Resolution Neutron Microtomographic Imaging. Frontiers in Ecology and Evolution, 2020, 8, 10.3389/fevo.2020.00042 . hal-02613789

HAL Id: hal-02613789
https://hal.science/hal-02613789

Submitted on 12 Nov 2020

HAL is a multi-disciplinary open access archive for the deposit and dissemination of scientific research documents, whether they are published or not. The documents may come from teaching and research institutions in France or abroad, or from public or private research centers.

L'archive ouverte pluridisciplinaire **HAL**, est destinée au dépôt et à la diffusion de documents scientifiques de niveau recherche, publiés ou non, émanant des établissements d'enseignement et de recherche français ou étrangers, des laboratoires publics ou privés.

frontiers in Ecology and Evolution

ORIGINAL RESEARCH
published: 27 February 2020
doi: 10.3389/fevo.2020.00042

When X-Rays Do Not Work. Characterizing the Internal Structure of Fossil Hominid Dentognathic Remains Using High-Resolution Neutron Microtomographic Imaging

Clément Zanolli[1], Burkhard Schillinger[2], Ottmar Kullmer[3,4], Friedemann Schrenk[3,4], Jay Kelley[5,6,7], Gertrud E. Rössner[8,9] and Roberto Macchiarelli[10,11]*

[1] Laboratoire PACEA, UMR 5199 CNRS, Université de Bordeaux, Pessac, France, [2] Heinz Maier-Leibnitz Center (FRM-II), Technische Universität München, Garching, Germany, [3] Department of Paleoanthropology, Senckenberg Research Institute and Natural History Museum Frankfurt, Frankfurt, Germany, [4] Department of Paleobiology and Environment, Institute of Ecology, Evolution, and Diversity, Goethe University Frankfurt, Frankfurt, Germany, [5] Institute of Human Origins, School of Human Evolution and Social Change, Arizona State University, Tempe, AZ, United States, [6] Department of Paleobiology, National Museum of Natural History, Smithsonian Institution, Washington, DC, United States, [7] Department of Human Evolutionary Biology, Harvard University, Cambridge, MA, United States, [8] SNSB-Bayerische Staatssammlung für Paläontologie und Geologie, Munich, Germany, [9] Department of Earth and Environmental Sciences, Palaeontology & Geobiology, Ludwig–Maximilians–Universität München, Munich, Germany, [10] UMR 7194 CNRS, Muséum National d'Histoire Naturelle, Musée de l'Homme, Paris, France, [11] Unité de Formation Géosciences, Université de Poitiers, Poitiers, France

OPEN ACCESS

Edited by:
Luca Pandolfi, University of Florence, Italy

Reviewed by:
Masato Nakatsukasa, Kyoto University, Japan
Amélie Beaudet, University of the Witwatersrand, South Africa

***Correspondence:**
Clément Zanolli
clement.zanolli@gmail.com

Specialty section:
This article was submitted to Chemical Ecology, a section of the journal Frontiers in Ecology and Evolution

Received: *13 January 2020*
Accepted: *11 February 2020*
Published: *27 February 2020*

Citation:
Zanolli C, Schillinger B, Kullmer O, Schrenk F, Kelley J, Rössner GE and Macchiarelli R (2020) When X-Rays Do Not Work. Characterizing the Internal Structure of Fossil Hominid Dentognathic Remains Using High-Resolution Neutron Microtomographic Imaging. Front. Ecol. Evol. 8:42. doi: 10.3389/fevo.2020.00042

The internal structure of the bones and teeth of extinct primates holds a significant amount of valuable paleobiological information for assessing taxonomy, phylogenetic relationships, functional, dietary and ecological adaptive strategies, and reconstructing overall evolutionary history. Technologies based on X-ray microfocus (X-μCT) and synchrotron radiation (SR-μCT) microtomography are increasingly used to non-invasively and non-destructively investigate the endostructural properties of fossil mineralized tissues. However, depending on the taphonomic dynamics that affected the specimens following deposition, and on the nature of diagenetic processes, X-μCT and even SR-μCT may provide only faint or no contrast between the mineralized tissues, thus complicating or inhibiting the study of structural features. Using a diverse sample of dentognathic hominid specimens from continental Asia, East Africa and Indonesia, chronologically ranging from the Late Miocene to the Early Middle Pleistocene, we present examples of the successful application of another imaging technology, neutron microtomography (n-μCT), for the extraction, 3D rendering and quantitative assessment of internal morphological detail. The specimens were scanned at the ANTARES Imaging facility (SR4a beamline) at the FRM II reactor of the Technical University of Munich, Germany, at energies ranging from 3 to 25 meV. The datasets were reconstructed with a voxel size from 20 to 27 μm, i.e., at resolutions directly comparable to the X-ray-based microtomographic records commonly used in paleobiological studies of fossil primate remains. Our analyses focused on a mandible, SNSB-BSPG 1939 X 4, representing the Late Miocene hominid *Sivapithecus* from the Siwaliks of Pakistan; the early Pleistocene

(Gelasian) partial mandible HCRP-U18-501 from Malawi, among the earliest specimens attributed to the genus *Homo*; and an assemblage of hominid dentognathic specimens from the Early Middle Pleistocene deposits of the Sangiran Dome, Indonesia. While X-ray-based imaging revealed from low to moderate internal contrasts for the specimen of *Sivapithecus*, or from extremely poor to virtually no contrast for the Pleistocene remains from East Africa and Indonesia, the application of n-μCT produced sufficient differences in contrast to distinguish between tooth tissues on the one hand, and between cortical and trabecular bone on the other, thus enabling reliable qualitative and quantitative assessments of their characteristics.

Keywords: neutron microtomography, micromorphology, mineralized tissues, taphonomy, diagenesis, paleoanthropology

INTRODUCTION

Before radiation-based analytical methods were made available for paleobiological research, the only way to extract information from the internal structure of fossils was to either study naturally broken remains, or to physically section specimens. Shortly after the discovery of X-rays by Röntgen (1895), plain radiography was first used in paleoanthropology to image some Neanderthal and Upper Paleolithic human dentognathic remains from Belgium (La Naulette, Goyet), Croatia (Krapina), Germany (Mauer), and Moravia (Pøedmostí) (Walkhof, 1902; Gorjanović-Kramberger, 1906; Schoetensack, 1908). Among other anatomical details, radiography revealed that the Neanderthal cheek teeth commonly bear an enlarged pulp cavity associated with pyramidal (or prismatic) roots (Gorjanović-Kramberger, 1906, 1907), a distinctive Neanderthal feature subsequently termed "taurodontism" (Keith, 1913).

Since these pioneering studies that revealed previously unreported dental and bony features, X-ray imaging has increasingly been used in paleobiological and paleoanthropological research, sometimes through the application of derivative techniques such as xeroradiography and multiple projection (stereo) X-rays (e.g., Meschan et al., 1979). However, plain film radiography generates two-dimensional (2D) synthetic images of the hidden anatomy resulting from the superimposition of overlying three-dimensional (3D) structures, which, depending on the volume of the investigated specimen, are limited in the extraction of subtle information from complex architectures, especially in fossils (Skinner and Sperber, 1982). The invention of X-ray computed tomography (CT; Hounsfield, 1973, 1975) provided for the first time the possibility to derive from the same object, and to treat separately and/or cumulatively, a series of cross-sectional images each taken on a distinct plane, thus avoiding the superimposition effect.

Medical CT scanning techniques led to new and exciting perspectives in paleontology and paleoanthropology, with the first applications of 3D imaging to fossil hominin remains dating to the 1980s (e.g., Tate and Cann, 1982; Wind, 1984; Conroy and Vannier, 1985, 1987; Zonneveld and Wind, 1985; Wind and Zonneveld, 1989). Often complemented by stereolithographic solid reconstructions, CT constituted the most effective technology to render inner structural variation at millimetric scale (rev. in Ulhaas, 2007; Macchiarelli et al., 2008; Braga, 2016). This remarkable methodological advance in 3D imaging enabled virtual access to previously infrequently investigated structures, such as the complete morphology of the bony labyrinth, which provided original information about locomotor behaviors and phylogenetic relationships (Spoor et al., 1994), and also allowed quantitative assessment of many other functionally related cranial and postcranial features (e.g., Jungers and Minns, 1979; Trinkaus, 1984; Ruff and Leo, 1986; Daegling, 1989). CT imaging also allows virtual reconstruction of broken and/or distorted areas through techniques of mirroring and interpolation, as well as by shape retro-deformation using morphometric approaches (e.g., Zollikofer and Ponce de León, 2005; Weber and Bookstein, 2011).

Nonetheless, even CT imaging has certain intractable limitations when analyzing highly mineralized specimens and/or specimens filled/surrounded by a dense sedimentary matrix, resulting from insufficient contrast among various structural components (e.g., mineralized tissues, infill, "empty" spaces/air) (Spoor et al., 2000). Overflow artifacts may also appear when the density of a specimen is greater than the scale maximum of the CT scan (i.e., when the signal received exceeds the dynamic range of the detector). Additionally, beam hardening – due to the absorption of low−energy X−rays leaving mostly high−energy photons – may result in overflow artifacts with saturated contrasts on the borders or in the densest areas (Spoor et al., 2000; Ulhaas, 2007). Depending on taphonomic history, fossils that have incorporated high-density elements (like iron) show streak artifacts on the CT images (Spoor et al., 2000). If the CT number scale is not fully adapted, as frequently occurs, or if no recalibration is applied, the resulting images have no contrast and altered thresholds. However, by using *ad hoc* filters, software and algorithm calibration, in most cases these kinds of problems can be minimized, if not fully overcome (Spoor et al., 2000; Ulhaas, 2007).

While CT scanning is still used to image relatively large fossil specimens and blocks of sedimentary breccia (e.g., Wu and Schepartz, 2009; Smilg and Berger, 2015), for smaller anatomical elements, like teeth and dentognathic fragments, the level of detail in digital reconstructions based on CT data is limited by the spatial resolution in the scan plane, slice thickness, and slice increment (for recent applications, see Beaudet et al., 2015;

Zanolli et al., 2017a). Indeed, with conventional CT scans it is possible to attain a final voxel size of only a few hundred micrometers (μm), while cone beam CT instruments (CBCT) reach resolutions near 100 μm but generate noisy images (Maret et al., 2014).

In the hominid fossil record, dentognathic remains are the most commonly preserved elements (Wood, 2011). Recent advances in the genetics and development of mineralized tissues demonstrate that the internal morphological structure of tooth crowns and roots bears a wealth of valuable taxon-specific biological information stored at a micrometric scale (Hillson, 2014; Guatelli-Steinberg, 2016; Scott et al., 2018; see also Smith and Tafforeau, 2008). Thus, given the conflicting requirements of preservation versus scientific exploitation of the fossil record, higher resolution non-invasive investigative techniques other than medical CT scanning are needed to safely but satisfactorily access the endostructural record (rev. in Macchiarelli et al., 2008).

X-ray microtomography (X-μCT) enabling the study of 3D features at micrometer scale was invented in the 1980s (Elliott and Dover, 1982). The results of the first applications of industrial X-μCT equipment to image the 3D endostructure of fossil hominoid (the Late Miocene ape *Oreopithecus*) and hominin (*Australopithecus*) teeth were published in 2004 (Macchiarelli et al., 2004; Rossi et al., 2004, respectively). These were quickly followed by the development of synchrotron radiation microtomography (SR-μCT), a highly effective analytical tool to detail meso/microscopic features (see Tafforeau et al., 2012), including dental endostructural morphology in extinct hominids (e.g., Macchiarelli et al., 2006, 2007, 2008; Mazurier et al., 2006; Tafforeau et al., 2006; Smith and Tafforeau, 2008; Tafforeau and Smith, 2008; Smith et al., 2009; Le Cabec et al., 2015). High-resolution X-μCT and SR-μCT have now become indispensable tools for the virtual exploration, extraction, cleaning, 2-3D rendering and quantitative assessment of the paleobiological information stored in fossilized remains (among the very many studies, see Rook et al., 2004; Olejniczak and Grine, 2005, 2006; Olejniczak et al., 2008; Skinner et al., 2008, 2015, 2016; Bayle et al., 2009, 2011; Macchiarelli et al., 2009, 2013; Braga et al., 2010; Kupczik and Hublin, 2010; Benazzi et al., 2011a,b; Jaeger et al., 2011; DeSilva and Devlin, 2012; Puymerail et al., 2012a,b; Zanolli et al., 2012, 2014, 2015, 2018a,b; Barak et al., 2013; Le Cabec et al., 2013; Zanolli and Mazurier, 2013; Spoor et al., 2015; Zanolli, 2015; Kappelman et al., 2016; Kivell, 2016; Macchiarelli and Zanolli, 2017; Martínez de Pinillos et al., 2017; Pan et al., 2017; Beaudet et al., 2018; Martín-Francés et al., 2018; Ryan et al., 2018; Beaudet, 2019; Cazenave et al., 2019a,b; Genochio et al., 2019; Grine et al., 2019; Haile-Selassie et al., 2019; Kupczik et al., 2019; Martinón-Torres et al., 2019; Pan and Zanolli, 2019).

Nevertheless, depending on the degree of alteration affecting specimens during fossilization, especially the impact of diagenesis, X-ray analyses of dental tissues do not always provide a distinct structural signal, thus sometimes limiting access to and extraction of information, or resulting in the recovery of no information whatsoever (Zanolli et al., 2017b). While X-μCT or SR-μCT usually make it possible to focus on local regions of interest (ROIs), or to use selected individual virtual slices to assess certain internal features (e.g., Smith et al., 2009, 2018; Skinner et al., 2013, 2015; Zanolli et al., 2015), there are also instances in which there is insufficient tissue contrast to allow reliable measurement, thus inhibiting the analysis of volumes of interest (VOIs).

Recently, a new investigative tool has become available to successfully detail the internal structure of fossil remains, neutron microtomography (n-μCT). Although neutrons were discovered in the 1930s and neutron radiography was applied for the first time to investigate fossil hominin remains already in the late 1990s (Le Roux et al., 1997), the exploitation of their physical characteristics in 3D imaging developed only when high quality neutron sources and detector systems became available (Tremsin et al., 2011). Neutrons have an absorption profile (interaction mechanism with matter) that differs from that of X-rays (Kardjilov et al., 2003; Winkler, 2006; Sutton, 2008; Tremsin et al., 2015). Because of a unique capacity of neutrons to penetrate materials opaque to X-rays, neutron-based analytical techniques such as neutron radiography and n-μCT represent highly effective tools for imaging fossil remains, often times providing adequate contrast resolution when other methods fail to do so (Zanolli et al., 2017b).

Following on the pioneering application of n-μCT to the analysis of fossil primate cranial and dental remains (Beaudet et al., 2016; Urciuoli et al., 2017; Zanolli et al., 2017b, 2019a), here we detail a series of cases illustrating the formidable potential of this analytical tool in the study of densely mineralized hominid dentognathic remains from different time periods and geographic contexts.

MATERIALS AND METHODS

Specimens

To illustrate different examples where X-ray-based imaging does not deliver a satisfying structural signal whereas n-μCT does, we selected an *ad hoc* assemblage of six hominid dentognathic remains chronologically ranging from the Late Miocene to the Early Middle Pleistocene, all from open-air sites in continental Asia, Africa and Indonesia.

The first specimen is a partial mandible of the late Miocene hominid *Sivapithecus*, from the Siwaliks of Pakistan. This genus exhibits a number of craniofacial similarities with extant orangutans and is considered to be related to *Pongo* (Pilbeam, 1982; Ward and Brown, 1986). However, *Sivapithecus* also displays features that are unlike those of *Pongo*, including dentognathic morphology (Kelley, 2002). We examined the left mandibular corpus, bearing two premolars and two molars, of the adult specimen SNSB-BSPG 1939 X 4, the holotype of *S. parvada*, from c. 10 million years (Ma) old levels of the Potwar Plateau (Dehm, 1983; Kelley, 1988, 2002). *S. parvada* is nearly twice the size of the two other common species of *Sivapithecus*, *S. indicus* and *S. sivalensis* (Dehm, 1983; Kelley, 1988, 2002). Resolving its relationships with the other *Sivapithecus* species, as well as clarifying its phylogenetic position with respect to *Pongo*, remain open research topics for which the extraction of additional dentognathic endostructural features could add

potentially relevant information. The specimen SNSB-BSPG 1939 X 4 is stored at the Bavarian Natural History Collections – Bavarian State Collection of Palaeontology and Geology, Munich, Germany.

We also examined the Early Pleistocene (Gelasian) partial mandible of an adult individual, HCRP-U18-501 (hereafter UR 501), found in 1991/92 at the Uraha site, Malawi (Schrenk et al., 1993). It comes from the stratigraphic Unit 3A of the Chiwondo Beds, Karonga Basin, biochronologically dated to 2.3–2.5 Ma (Kullmer, 2008). This is an especially relevant time period in hominin evolution as it corresponds to the emergence and initial diversification of the genus *Homo* (Villmoare, 2018). UR 501 consists of two joined parts of the corpus broken on both sides behind the m2s, but preserving the p3-m2 tooth sequence. We analyzed the X-μCT and n-μCT records of the right portion. The size and proportions of this specimen, the symphyseal shape, the anteroposteriorly elongated dental arcade, and details of external tooth morphology show remarkable similarities with the specimen KNM-ER 1802 from Koobi Fora, Kenya, regarded as representing *Homo* cf. *habilis*, as well as with OH 7 from Olduvai Gorge, Tanzania, the holotype of *H. habilis* (Spoor et al., 2015). However, it also possesses some *Australopithecus*-like as well as unique features, a mosaic which makes the taxonomic placement of this fossil challenging. Thus, any diagnostic information deriving from the analysis of its endostructure has the potential of contributing to a more definitive taxonomic assignment, and therefore better assessment of its likely affinities (Zanolli et al., 2019b). The mandible UR 501 is stored at the Senckenberg Museum of Frankfurt am Main, Germany.

We also selected an assemblage of four hominid dentognathic remains from the Early Middle Pleistocene deposits of the Sangiran Dome, Java, Indonesia. These include the right mandibular portion of Sangiran 6a, the holotype of *Meganthropus palaeojavanicus* (Weidenreich, 1945; von Koenigswald, 1950), as well as the isolated hominid permanent lower molars Sangiran 7–20, Sangiran 7–65, and SMF-8888, all of whose taxonomic attribution to *H. erectus*, *Meganthropus* or even *Pongo* remain uncertain. Indeed, Indonesian hominid diversity across the Pleistocene has been a matter of contention for over a century (rev. in Zanolli et al., 2019a). Due to the marked morphological and metric variation characterizing the larger fossil assemblage from which these specimens derive, some robust specimens from Sangiran have been alternatively allocated to various hominid taxa (e.g., *Pithecanthropus dubius*, *Meganthropus palaeojavanicus*, *Pongo* sp.) (von Koenigswald, 1950; Tyler, 2004). More recently, the variation displayed by the Indonesian assemblage has also been regarded as being compatible with a single taxon, *Homo erectus* (e.g., Kaifu et al., 2005). In contrast, new analyses of the endostructural signature virtually extracted from some of the Sangiran specimens using a combination of X-μCT, SR-μCT, and n-μCT have revealed a higher level of taxonomic diversity than previously recognized, thus supporting the validity of the taxon *Meganthropus*, an ape that coexisted during the Early to Middle Pleistocene in the region with *H. erectus*, *Pongo* and, perhaps, also *Gigantopithecus* (Zanolli et al., 2019a). All fossils from the Sangiran Dome formations considered in this study are stored at the Senckenberg Research Institute and Natural History Frankfurt in Frankfurt am Main, Germany.

Methods of Analysis

The left portion of the mandible SNSB-BSPG 1939 X 4, the right portion of the mandible UR 501 and the four dentognathic specimens from Sangiran (Sangiran 6a, Sangiran 7–20, Sangiran 7–65, and SMF-8888) were scanned between 2016 and 2018 at the ANTARES imaging facility located at the FRM II reactor of the Technical University of Munich, Germany. The facility operates on one channel (of two) of the cold neutron beamline SR4, being the only cold neutron imaging facility at a reactor with direct sight to the cold source with neutron flight tubes instead of neutron guides. Due to this architecture, neutrons travel on a straight flight path and do not lose collimation and spectral homogeneity by reflection on neutron guides. There are two chambers containing sample and detector positions, one for samples up to 15 cm in size, and another one for larger samples up to 30 cm (Schillinger et al., 2018).

The neutron beam originates from the cold source of the FRM II reactor with an energy range mostly from 3 to 25 meV, a collimation ratio of L/D = 500 (the ratio between the sample-detector distance and collimator aperture), and an intensity of 6.4×10^7 n/cm^{2}s. A 20 μm Gadox screen was used to detect neutrons. Both a cooled, charge-coupled device camera (ikon-L 936; Andor) and a cooled complementary metal-oxide semiconductor camera (Neo 5.5 sCMOS; Andor) were used as detectors. The final virtual volume of the analyzed specimens was reconstructed with an isotropic voxel size of 20–27 μm, i.e., at resolutions directly comparable to the X-ray-based microtomographic records commonly used in studies of fossil primate teeth.

All specimens were also preliminarily imaged by X-μCT at comparable resolutions (**Table 1**). For two of them, Sangiran 7–20 and Sangiran 7–65, a SR-μCT record was produced at the European Synchrotron Radiation Facility of Grenoble, France, within the context of another independent study (Smith et al., 2018) and made available online[1].

Because in both X-μCT and n-μCT the detection of the tissue interfaces is based on attenuation at the boundary of the target, we performed a threshold-based segmentation as usually applied for X-ray acquisitions (Beaudet et al., 2016; Zanolli et al., 2017b; Schillinger et al., 2018). Due to parallel beam geometry and much lower source intensity with respect to X-ray-based analyses (the neutron beam contains about three to five orders of magnitude fewer particles than an X-ray or synchrotron beam contains photons), the reconstructed n-μCT images are generally noisier than those obtained at comparable spatial resolutions by X-μCT or SR-μCT (**Figure 1**) with much higher counting statistics. Thus, a median filter with a kernel size of 2–3 was applied to the n-μCT records both prior to and during the segmentation process, and manual corrections were also locally applied to eliminate the remaining artifacts (Zanolli et al., 2017b, 2019a; Schillinger et al., 2018). A previous test performed on a fossil hominid tooth on

[1] http://paleo.esrf.fr

TABLE 1 | Acquisition parameters of the X-μCT and n-μCT records of the specimens used in this study.

Specimen	Chronology	Origin	X-μCT					n-μCT			
			Instrument	Voltage	Current	Filter	Projections	Voxel size	Energy range	L/D collimation ratio	Intensity	Voxel size
SNSB-BSPG 1939 X 4	Tortonian	Pakistan	Nanotom m	140 kv	0.02 mA	0.2 mm Cu	1400	51.9 μm	3–25 meV	500	6.4 × 10^7 n/cm^2s	27.1 μm
HCRP-U18-501	Gelasian	Malawi	BIR SN001	150 kV	0.11 mA	0.5 mm brass	5000	32.8 μm	3–25 meV	500	6.4 × 10^7 n/cm^2s	26.0 μm
Sangiran 6a	Early Middle Pleistocene	Java	BIR SN001	150 kV	0.11 mA	0.5 mm brass	5000	39.3 μm	3–25 meV	500	6.4 × 10^7 n/cm^2s	20.5 μm
Sangiran 7–20	Early Middle Pleistocene	Java	Skyscan 1172	100 kV	0.10 mA	Al + Cu	3000	13.7 μm	3–25 meV	500	6.4 × 10^7 n/cm^2s	19.5 μm
Sangiran 7–65	Early Middle Pleistocene	Java	Skyscan 1172	100 kV	0.10 mA	Al + Cu	1800	27.5 μm	3–25 meV	500	6.4 × 10^7 n/cm^2s	22.0 μm
SMF-8888	Early Middle Pleistocene	Java	Nanotom	100 kV	0.07 mA	none	1800	25.8 μm	3–25 meV	500	6.4 × 10^7 n/cm^2s	21.7 μm

*Acquisition parameters of the SR-μCT data are detailed below the table (see asterisk). *The SR-μCT records of Sangiran 7–20 and Sangiran 7–65 were downloaded from the European Synchrotron Radiation Facility Paleontological Microtomographic Database (see text footnote 1). These specific data were acquired on beamline ID 19 at the European Synchrotron Radiation Facility (ESRF, Grenoble, France), with an average energy of 68.3 keV filtering the white beam of the ID19 W150 wiggler set at a gap of 35 mm by 3 mm of aluminum, 0.25 mm of copper and 0.06 mm of tungsten, using a FReLoN 2K14 CCD camera in frame transfer mode, a 24 μm thick GGG:eu scintillator, and 5000 projections of 0.3 s each in half-acquisition mode (Smith et al., 2018). The final dataset was generated with a voxel size of 4.96 μm, then downsampled to 20 μm for comparison with the n-μCT data.*

FIGURE 1 | Comparison between the X-μCT- **(A)** and n-μCT-based **(B)** virtual sections through the mesial cusps of a modern human maxillary M3. The enamel (light gray) – dentine (dark gray) boundary is distinctly traceable in both cases. The total acquisition times to scan the specimen were of 120′ (X-μCT) and 22 h (n-μCT).

the degree of coherence between the X-μCT and n-μCT data sets showed average volume differences <5% (Zanolli et al., 2019a).

RESULTS

Both the X-μCT and n-μCT records of the *Sivapithecus parvada* mandible SNSB-BSPG 1939 X 4 provided relatively good contrast between enamel and dentine tissues (**Figure 2**). For example, in both records the linear measure of the maximal cuspal enamel thickness assessed here at the protoconid cusp of the m2 (**Figure 2**) ranges from 1.68 to 1.75 mm. However, X-ray- and neutron-based imaging do not systematically render the same structural information. As imaged by X-rays, the internal structure of the mandibular corpus appears as nearly uniform gray, while relevant details are revealed by the neutron record (**Figures 2C,D**). In the latter case the endosteal perimeter can be confidently traced and the distinction among cortical shell, trabecular bone and matrix infill can be discerned, thus allowing assessment of topographic variation in cortical bone thickness and, at least at some site-specific ROIs and limited VOIs, assessment of 2-3D local textural properties of the cancellous

FIGURE 2 | 3D virtual rendering of the *Sivapithecus parvada* left mandibular corpus, SNSB-BSPG 1939 X 4, in lingual **(A)** and occlusal **(B)** views. The longitudinal virtual sections through the corpus [orange line, in **(B)**] were extracted from the X-μCT **(C)** and n-μCT **(D)** records, respectively. The dotted white line in **(D)** shows the endosteal margin of the cortical bone, not visible in **(C)**.

network, such as strut thickness and orientation. The neutron record also much more clearly reveals the multiple breaks affecting the molar roots, especially those of the m2, evidence hardly appreciable on the entire set of related X-μCT-based slices. In paleobiological research, qualifying and quantifying the degree of internal taphonomic alteration is critical, particularly when planning for potentially invasive sampling.

Additional differences between the two records of SNSB-BSPG 1939 X 4 are evident by comparing the virtual sections through the mesial m2 cusps (**Figure 3**). While both imaging types show similar contrasts between enamel and dentine, the X-μCT reveals poor contrast between bone and radicular dentine and, in addition to failing to render root cracking, also masks the extent of bone micro-fragmentation between the roots, a feature distinctly unveiled by n-μCT (**Figures 3A,B**). It is noteworthy that, besides more easily penetrating denser materials generally opaque to X-rays, neutrons also actively interact with light chemical elements, such as hydrogen or lithium (Tremsin et al., 2015), occurring in the glues commonly used to fix broken specimens, or in the varnishes formerly employed to coat the fossils. In the case of SNSB-BSPG 1939 X 4, the interaction of neutrons with these light elements is revealed by brighter areas such as those occurring along the breakages present at the base of the m2 crown, originally consolidated by glue (**Figure 3B**); this information is missing in the corresponding X-μCT image (**Figure 3A**).

The partial mandible UR 501 from Malawi and virtual sections through its right m1 are shown in **Figure 4**. In this densely mineralized specimen, X-μCT reveals only faint contrasts between bone and dentine, while the endosteal contour of the cortical bone is distinguishable from the homogenized inner cancellous network and sedimentary matrix (**Figure 4C**). However, no distinction is discernable between enamel and dentine. This is likely due to a combination of factors, including remineralization of the dental tissues during fossilization and the taphonomic inclusion of heavy elements absorbing part of the X radiation, a phenomenon visible as saturation overflow in the X-μCT images (**Figure 4C**). Using the X-μCT record, a recent study tentatively segmented and imaged the m2 pulp chamber, but the result is incomplete (Kupczik et al., 2019: **Figure 4B**). In contrast, n-μCT distinctly distinguishes cortical bone from the sedimentary matrix and also reveals some details of the porous cancellous network (**Figure 4D**). The conformation of the enamel-dentine junction (EDJ) of the p4 and first two molars, useful in taxonomic comparisons among extinct hominids (Skinner et al., 2008, 2016; Zanolli et al., 2012, 2014, 2019a; Macchiarelli et al., 2013; Pan et al., 2017), can also be visualized and confidently assessed (**Figure 5**).

Both X-μCT and n-μCT of Sangiran 6a from Early Pleistocene Java revealed good contrast between the m1 enamel and dentine (**Figures 6A,B**). This permitted two independent segmentations of this specimen to compare measurements of 3D virtual EDJ surfaces. Our repeated tests show that, when superimposing the X-μCT- and n-μCT-based surfaces, the differences do not exceed the 240 μm distance between the faces of each surface, with an average of 65.7 μm (Zanolli et al., 2019a). Considering the difference in voxel size between the original records (39.3 and

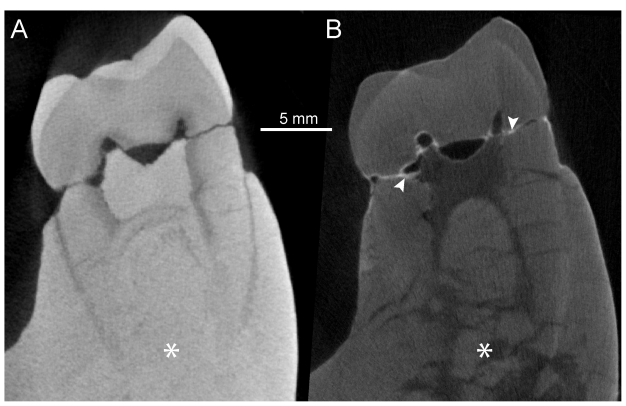

FIGURE 3 | X-μCT- **(A)** and n-μCT-based **(B)** virtual sections through the mesial cusps of the left m2 of SNSB-BSPG 1939 X 4 (*S. parvada*). The white arrows in **(B)** highlight areas where lighter elements contained in the glue originally used to consolidate the specimen absorbed more neutrons, thus generating a whiter fringe along the fractures. The asterisks, respectively, indicate **(A)** the lack of structural signal in the X-μCT section and **(B)** the actual degree of bone and radicular micro-fragmentation uniquely revealed by n-μCT imaging.

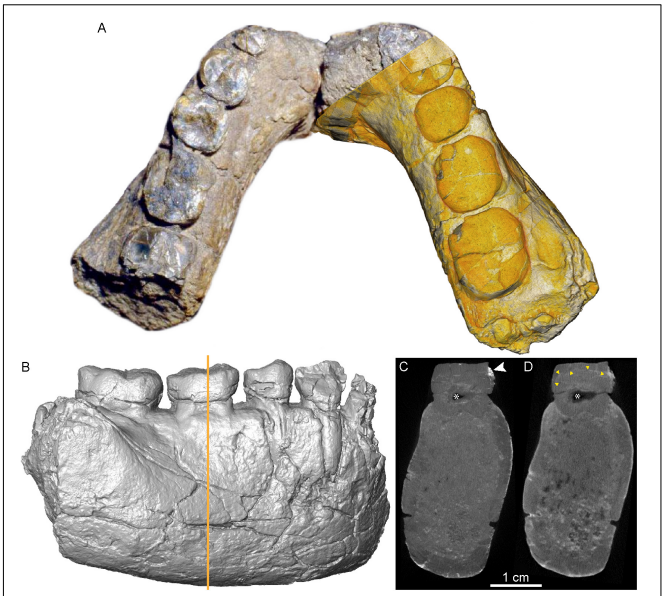

FIGURE 4 | Photomontage of the UR 501 hominin mandible, with the n-μCT-based 3D rendering virtually superimposed over the right portion **(A)**. The X-μCT-based rendering of the same portion in buccal view is shown in **(B)**. The coronal virtual sections through the corpus [orange line in **(B)**] were respectively, extracted from the X-μCT **(C)** and the n-μCT **(D)** records. The white arrow in **(C)** highlights a denser area that absorbed more X-rays, creating a local saturation overflow that overwhelms the rest of the contrast range, thus reducing contrasts between enamel and dentine. The yellow arrow heads in **(D)** indicate the enamel-dentine boundary, not visible in **(C)**. The asterisks in **(C)** and **(D)** show differences in imaging of the pulp chamber, which is partially infilled with sediment (nearly transparent in the neutron analysis).

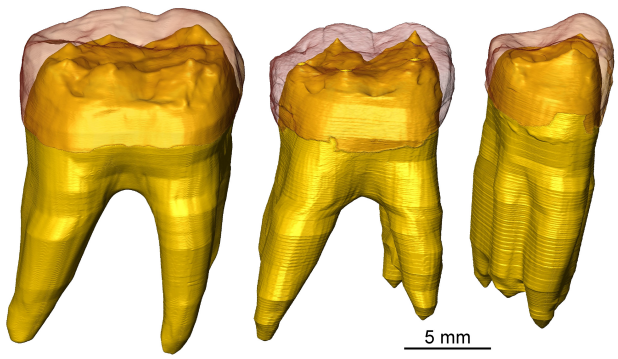

FIGURE 5 | n-μCT-based 3D surfaces of the virtually extracted right p4, m1, and m2 of the UR 501 mandible, with the reddish enamel in semi-transparency revealing details of the EDJ and the crown and radicular dentine rendered in yellow.

20.5 μm for, respectively, X-μCT and n-μCT), such differences can be considered as negligible. In fact, measurements of the enamel and crown dentine volumes (the latter including the crown pulp), show differences of <3 μm^3, which represents less than 1% of the respective volumes (Zanolli et al., 2019a). This demonstrates a high level of concordance between the X-ray- and neutron-based records, even in the rendering of micro-features such as details of the EDJ morphology (**Figures 6C–F**).

However, due to diagenetic changes, only a fraction of dentognathic fossil specimens imaged by industrial X-μCTs provide results as satisfactory as those obtained on Sangiran 6 (e.g., Olejniczak and Grine, 2006; Zanolli et al., 2015, 2019a). This is true for a large majority of the Early Middle Pleistocene isolated hominid teeth from Java, for which X-μCT records of endostructural features are largely unsatisfactory (Smith et al., 2009; Zanolli et al., 2017b, 2019a; Schillinger et al., 2018), and for which interfaces among enamel, dentine, bone and sediment are sometimes difficult to distinguish. The same is true even using SR-μCT (Smith et al., 2009, 2018). This was also found to be the case with the three isolated lower molars from the Sangiran Dome considered in this study.

The X-μCT scan of the lower molar crown SMF-8888 resulted in a rather homogeneous gray signal, with no contrasts among the subocclusal structures (**Figure 7A**). Conversely, the n-μCT record of this specimen unambiguously distinguishes between enamel and dentine, and also reveals the shape of the pulp horns, barely perceptible on the X-ray images (**Figure 7B**). Similarly, the original X-μCT record of the lower molar Sangiran 7–20 showed no internal contrasts, whereas the SR-μCT scan revealed some tissue-related density differences (**Figure 8A**). However, the contrasts are moderate and there are a number of marginal bright areas resulting from phase contrast imaging that make the segmentation of dental tissues arduous (Smith et al., 2018; see SR-μCT data available at http://paleo.esrf.eu/picture.php?/3229/category/2223). Despite the presence of some noise in the

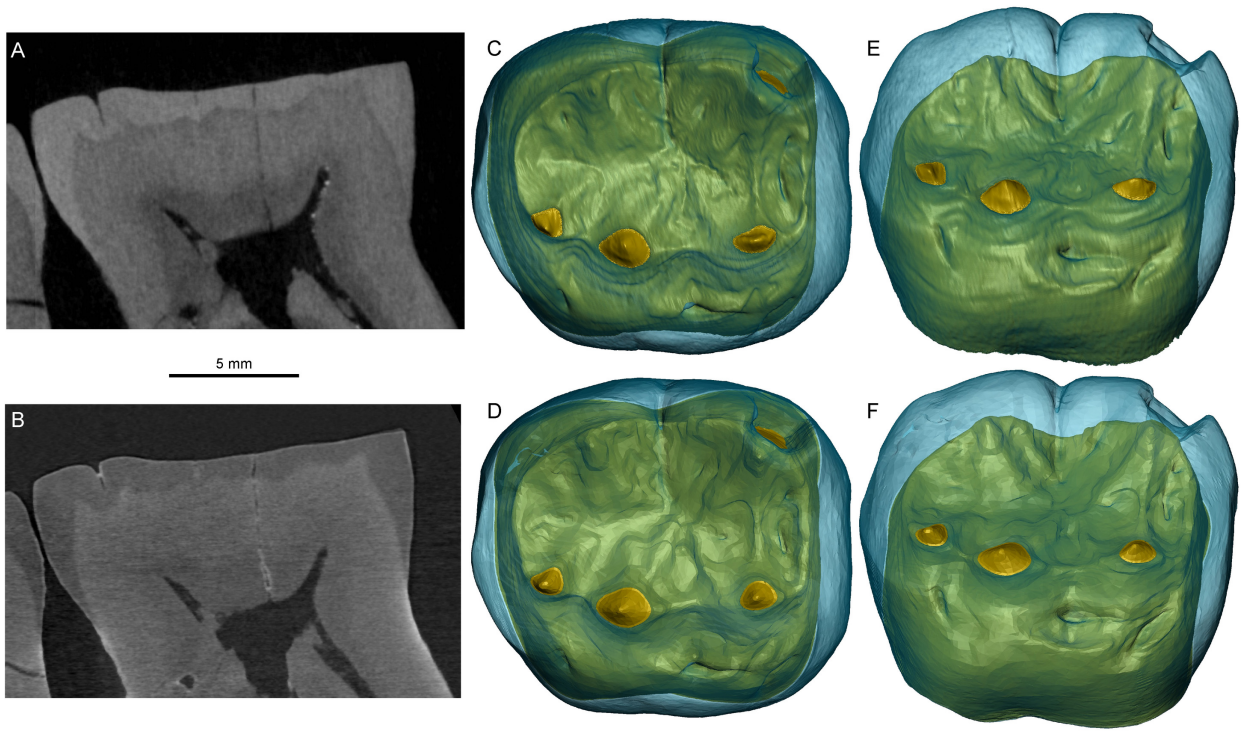

FIGURE 6 | X-μCT- **(A)** and n-μCT-based **(B)** mesiodistal virtual sections through the middle of the right m1 of the Sangiran 6a mandible (*Meganthropus palaeojavanicus*). The 3D renderings of the crown, respectively, generated by the X-ray-based **(C,E)** and neutron-based **(D,F)** records are shown in occlusal **(C,D)**, and occlusobuccal **(E,F)** views.

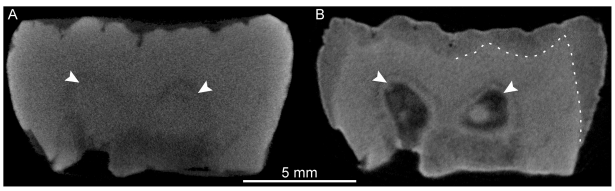

FIGURE 7 | X-μCT- **(A)** and n-μCT-based **(B)** mesiodistal virtual sections through the buccal cusps of the lower molar SMF-8888. The white arrows indicate the positions of two pulp horns barely discernible on the X-ray image **(A)** but clearly rendered by the neutron-based record **(B)**. The dotted line in **(B)** highlights the enamel-dentine boundary, not visible in **(A)**.

record, neutron imaging separates the darker gray enamel from the lighter gray dentine (**Figure 8B**). In contrast to the model generated from the original X-μCT record, the 3D surfaces, respectively, derived from SR-μCT (**Figure 8C**) and n-μCT (**Figure 8D**) are compatible in rendering subtle features of the EDJ, notably the five low but well-expressed dentine horns and the faint crests emanating from them. Finally, in the case of the lower molar Sangiran 7–65, neither the X-μCT nor SR-μCT records produced contrasts sufficient to distinguish enamel and dentine across the whole crown (**Figures 9A,B**). In some SR-μCT virtual slices the phase contrast fringes appearing along some fractures may even be confounded with the contour of the EDJ interface (**Figure 9B**). Misinterpreting these features would lead to the false assessment of extremely thick enamel in this specimen, reaching an apparent thickness of 2.08 mm at the level of the orange arrow in **Figure 9B**. Instead, as revealed by the neutron analysis, the EDJ contour (**Figure 9C**) is much nearer the enamel occlusal surface (**Figure 9D**), with actual enamel thickness at the same point being at most 1.15 mm.

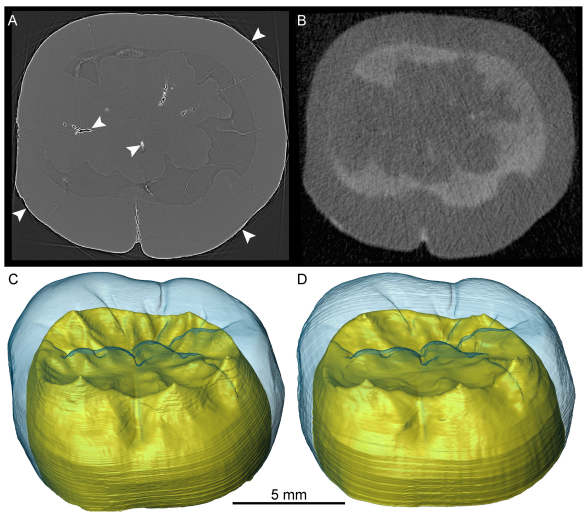

FIGURE 8 | SR-μCT- **(A)** and n-μCT-based **(B)** transverse virtual cross-sections of the crown of the lower molar Sangiran 7–20. The corresponding 3D surfaces are shown in **(C,D)**, respectively, where the blue enamel in semi-transparency reveals details of the EDJ and the crown dentine is rendered in yellow. The white arrows in **(A)** show the bright fringes produced by the phase contrast effect.

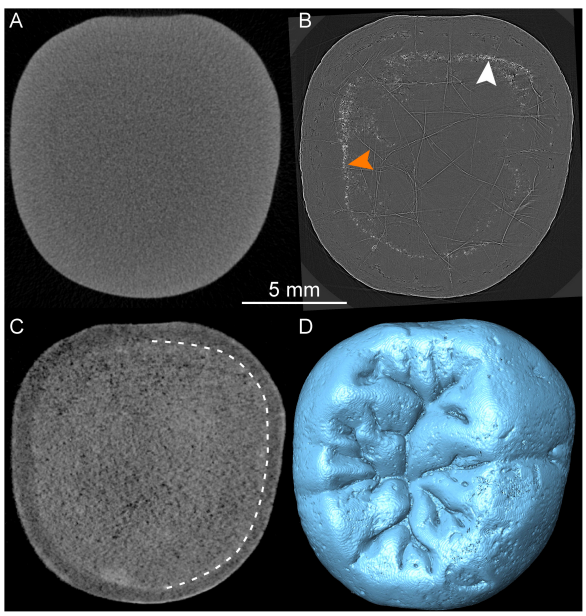

FIGURE 9 | X-μCT- **(A)**, SR-μCT- **(B)**, and n-μCT-based **(C)** transverse virtual cross-sections of the crown of the lower molar Sangiran 7–65. The SR-μCT-based 3D rendering of the crown occlusal morphology is shown in **(D)**. The white and orange arrows in **(B)** show the bright fringes produced by the phase contrast effect. The dotted line in **(C)** indicates the enamel-dentine boundary, not visible in **(A)** (X-μCT) or **(B)** (SR-μCT).

DISCUSSION

Industrial X-μCT instruments are now increasingly available for routine analyses in national museums and research institutions and are generally regarded as the best-suited tool for the non-invasive and non-destructive examination, and virtual "immortalization," of cultural heritage and fossil remains (Macchiarelli and Weniger, 2011). However, as commonly experienced by researchers investigating highly re-mineralized specimens, SR-μCT phase-contrast imaging may be a much more effective analytical tool (Paganin and Pellicia, 2019), capable of rendering subtle details even at infra-micrometric scale (e.g., Le Cabec et al., 2015, 2017; Smith et al., 2015, 2018; Xing et al., 2019). The recent use of n-μCT in paleoanthropology is revealing new and exciting opportunities for examining fossil specimens of higher density whose inner structural organization cannot be satisfactorily rendered by X-ray-based equipment (Beaudet et al., 2016; Urciuoli et al., 2017; Zanolli et al., 2017b, 2019a; Schillinger et al., 2018).

With X-μCT and SR-μCT, imaging contrasts among different materials result from the interactions of the X-rays with the electrons of the target (i.e., photoelectric and Compton effects), which depend on the atomic number of its elements. The contrasts obtained by X-rays are due to different natural absorption and scattering properties of the analyzed materials,

and to the different electron cloud densities surrounding the atoms within them (Winkler, 2006; Sutton, 2008). Thus, in the case of densely re-mineralized specimens, X-rays might be highly absorbed and thus deliver weak contrast signals (e.g., Skinner et al., 2013, 2015; Zanolli et al., 2015). Since neutrons, as neutral particles, are only absorbed or scattered by the nucleus of the atom, this does not apply to neutron-based analyses. n-μCT's imaging contrast depends only on the composition of the nuclei in the sample, often showing high attenuation (absorption and scattering) differences between neighboring elements, and even between isotopes of the same element (Kardjilov et al., 2003; Winkler, 2006; Tremsin et al., 2015). While enamel and dentine are originally mainly composed of hydroxyapatite $[Ca_{10}(PO_4)_6(OH)_2]$, they also integrate different proportions of organic matter and water that are almost always eliminated in fossil specimens and eventually replaced by various elements during diagenesis. Therefore, it is likely the differences in composition of hydroxyapatite in the mineralized dental tissues that are mostly responsible for the different contrasts in the virtual images. Hydrogen is a special case, as it attenuates neutron beams by equal-mass scattering. This is why glues and coatings that contain a high level of hydrogen (and other light elements) appear well-visible in neutron analyses (see **Figure 3**). For this reason, and because they could also affect future biomolecular analyses, chemical products should be used sparingly when preparing and restoring fossils (Le Cabec and Toussaint, 2017).

Compared with X-rays, neutrons also have the ability to penetrate materials with minimal attenuation (Tremsin et al., 2015) and are thus well-suited to analyze the internal structure of geological and paleontological samples, especially to distinguish between mineralized tissues and matrix (Schwarz et al., 2005; Sutton, 2008; Beaudet et al., 2016; Zanolli et al., 2017b; Schillinger et al., 2018). With recent advances in hardware and beamline settings, n-μCT can now reach a resolution of <5 μm, closing the gap with X-μCT instruments. In any case, neutron analyses deliver high imaging contrasts different from those of X-rays, and are therefore complementary (Sutton, 2008). In addition, the very low energies of cold neutrons and consequent weak interactions with matter make them penetrative and non-destructive, including for organic matter like DNA and proteins (Lakey, 2009). Thus, compared with SR-μCT, which can affect DNA preservation in fossil samples (Immel et al., 2016), n-μCT represents a very safe approach to investigate the internal structure of biological and fossilized materials without damaging the potentially preserved organic molecules.

Even if neutron analyses represent a viable complement or alternative to X-ray investigations, they also have limitations and downsides. First, compared with availability of synchrotrons in many countries worldwide, there are only a handful of neutron facilities that can perform high-resolution n-μCT scans. These include ANTARES at the Technical University of Munich in Germany, ICON at the Paul Scherrer Institute in Switzerland, NEXT at the Institut Laue-Langevin in France, NIST at the National Institute of Standards and Technology in the United States, and DINGO at the Australian Nuclear Science and Technology Organisation in Australia (Lehmann, 2017; Schillinger et al., 2018), plus a few more emerging facilities. As is the case with synchrotrons, access to these n-μCT facilities is based on the acceptance of *ad hoc* scientific proposals following a solicitation, and beamtime is generally limited to a few days per year. A further limitation is that n-μCT acquisition for fossil material takes several hours, as the exposure time needs to be long-enough to record sufficient signal (on average, each scan performed in this study required 20 h with exposure times between 30 and 90 s/projection) and the number of needed projections to get a high resolution is quite large (877 projections in total for each analysis performed in this study). However, in contrast to X-rays, which are strongly absorbed by materials such as fossil mineralized tissues, with n-μCT several isolated specimens can be scanned simultaneously without losing contrast quality. For example, 10–20 isolated hominid teeth were scanned in each acquisition at ANTARES, including the three specimens from Sangiran illustrated here. Another important aspect to consider is the temporary increase of radioactivity of the material induced by the neutron radiation absorbed during n-μCT scanning. As proscribed by national and international radioprotection legislation, irradiated samples have to be kept on-site in radiation-proof safes until they return to the natural background level of radioactivity and are authorized to leave the facility. However, the level of radioactivity of the specimens just after an acquisition is low (a few tens to hundreds of μSv) and generally decreases quickly. In the last 5 years, some hundreds of fossils from various time periods, locations and geological contexts have been analyzed at ANTARES, and all came back to their natural radioactivity level after some days or a few weeks (on average, after 12–15 days) to then be returned to the institutions where they are permanently stored.

As demonstrated in this study, neutron imaging reveals structural information that is not always visible with X-rays. In the case of the Miocene specimen SNSB-BSPG 1939 X 4 attributed to *S. parvada*, enamel and dentine are well-distinguished on both X-μCT and n-μCT images, while the internal bone structure and its damages are only visible on the neutron record. Mandibular cortical bone thickness is partly linked with functionally related strains of mastication and feeding behaviors (see Genochio et al., 2019). Thanks to n-μCT, the assessment of cortical thickness is now possible in this specimen, and together with the study of teeth, its analysis will potentially reveal new information on the biomechanical adaptions and taxonomic-related features of this species.

Among the examples presented in this study illustrating the variable nature and quality of the endostructural signals comparatively rendered by X-ray- and neutron-based records, those of the partial mandibles UR 501 from Malawi, and Sangiran 6a from Java, deserve further comment because of the taxonomic implications of the results. As briefly mentioned, the 2.3–2.5 Ma specimen UR 501 shows outer morphological and dimensional affinities with both *Homo habilis* (e.g., OH 7 and KNM-ER 1802) and early *Homo* (e.g., KNM-ER 64060) remains (Spoor et al., 2015; Grine et al., 2019), while its plate-like premolar roots and some microanatomical features of the teeth resemble those of *Paranthropus* (Kullmer et al., 2011). Indeed, its taxonomic attribution (Schrenk et al., 1993) and that of the few other African earliest Pleistocene fossils regarded as potentially representing earliest members of the genus *Homo* is still debated (Wood and Boyle, 2016; Villmoare, 2018). As summarized in

Figures 4, **5**, the n-μCT imaging of UR 501 recently allowed the extraction of information from the postcanine dentition of this specimen previously unavailable on the basis of the X-μCT record. In particular, a comparative geometric morphometric (GM) analysis of the molar EDJ with representatives of the taxa *Australopithecus*, *Paranthropus*, and *Homo* now suggests that UR 501 may be more closely related to the australopiths than to *Homo* (Zanolli et al., 2019b). Combined with new paleoecological scenarios associated with the Malawian hominin fossil record (Lüdecke et al., 2018), these results highlight the complexities of the phylogenetic and biogeographic history of early *Homo* and stimulate the discussion about the emergence of our own genus.

Concerning Sangiran 6a, because of its especially large size and primitive morphology, it was originally attributed to the taxon *Meganthropus* (Weidenreich, 1945; von Koenigswald, 1950), but was shortly thereafter integrated into the growing *H. erectus s.s.* hypodigm (e.g., Kaifu et al., 2005). Indeed, following the discovery at Trinil in 1891 of *Pithecanthropus* (*Homo*) *erectus* by E. Dubois (1894), the taxonomic attribution of some of the most robust hominid specimens from Java became the object of intense debate for nearly a century, and the question of the hypothetical presence of a non-*Pongo* great ape penecontemporaneous with *H. erectus* in the region remained unanswered (Ciochon, 2009). In the case of Sangiran 6a, the combined use of X-μCT and n-μCT analyses unveiled details of internal structure demonstrating that, together with other robust Javanese remains, this specimen actually belongs to the non-hominin hominid *Meganthropus palaeojavanicus* (Zanolli et al., 2019a). However, for other isolated teeth from the Pleistocene of Indonesia, both X-μCT and even SR-μCT analyses failed to deliver sufficient contrast between tissues to confidently assess their characteristics (e.g., Smith et al., 2009, 2018). Conversely, as illustrated by the three specimens Sangiran 7–20, Sangiran 7–65, and SMF-8888, the n-μCT record illuminated critical qualitative and quantitative information invisible by X-ray imaging.

CONCLUSION

It is likely that the Miocene to Pleistocene available fossil record only samples a portion of actual hominid and hominin taxonomic paleodiversity (e.g., Haile-Selassie et al., 2016; Wood and Boyle, 2016). Thus, the importance of continually developing preferably non-destructive investigative methods capable of maximizing the information extracted from typically fragmentary and scattered remains. Recently developed advanced technologies now enable the high-resolution imaging and subtle characterization of both external and internal morphology of fossil specimens, assuring both a virtual repository of this fragile record and providing the capability of "virtual dissection" at unprecedented levels of detail. Thanks to progresses in hardware technologies, increases in computing power, the emergence of commercial and free software dedicated to the analysis of 3D data, and to the dissemination of universal formats and Internet facilities, it has become possible to store and share online databases and to easily exchange images and data from fossil specimens worldwide in real time, a genuine revolution in the traditionally parsed field of paleoanthropology (Rook et al., 2004; Macchiarelli et al., 2008, 2013; Macchiarelli and Weniger, 2011; Hublin, 2013; Skinner et al., 2013). In this realm, X-ray-based analytical tools remain the first choice for the study of fossil specimens, and their systematic use to build "digital archives" easily accessible to students and researchers worldwide should be encouraged and supported by *ad hoc* programs. However, whenever X-rays, given their limited penetration range, fail to render important endostructural details, neutron imaging represents a complementary and/or alternative analytical solution.

Following our ongoing examinations, we predict that the use of n-μCT will contribute in the near future to significantly increase the quality and amount of paleobiological information routinely extracted from the fossil record and, with special reference to dentognathic remains, will likely play a relevant role in answering questions about the taxonomic status of some still controversial specimens, including those potentially representing early *Homo*.

DATA AVAILABILITY STATEMENT

All data supporting the findings of this study are included in the article.

AUTHOR CONTRIBUTIONS

CZ, OK, FS, and RM designed the research. CZ, BS, OK, JK, and GR realized the *n*-μCT analyses of the fossil specimens. GR performed the X-μCT scan of SNSB-BSPG 1939 X 4. CZ performed the segmentation and extracted the data for this study. All authors contributed to the discussion and interpretation of the results. CZ and RM wrote the manuscript with contributions from all other authors.

FUNDING

FRM II measurements were supported by the European Commission under the 7th Framework Program through the "Research Infrastructures" action of the "Capacities" Program NMI3-II (grant number 283883). This project was produced with financial support from the French National Research Agency (ANR) under the Investments for the Future Scheme, within the LaScArBx Cluster (ANR-10-LABX-52).

ACKNOWLEDGMENTS

We thank the co-editors L. Pandolfi, L. Rook, P. Raia, and J. Fortuny for their kind invitation to contribute to this special volume "Evolving Virtual and Computational Palaeontology." We acknowledge the Bavarian Natural History Collections for access to its X-μCT instrument, and the Department of Human Evolution at the Max Planck Institute for Evolutionary Anthropology, Leipzig, for access to the comparative X-μCT records of the UR 501 mandible and Sangiran 7–20, Sangiran

7–65, and SMF-8888 isolated teeth. T. L. Kivell, C. B. Ruff, and E. Trinkaus kindly provided bibliographic information. We express our gratitude to the Werner Reimers Foundation in Bad Homburg, which provides the Gustav Heinrich Ralph von Koenigswald collection as a permanent loan for scientific research to the Senckenberg Research Institute and Natural History Museum Frankfurt. We also thank A. Beaudet for discussion. Finally, we gratefully acknowledge the financial support provided by FRM II to perform the neutron measurements at the Heinz Maier-Leibnitz Zentrum (MLZ), Garching, Germany.

REFERENCES

Barak, M. M., Lieberman, D. E., Raichlen, D., Pontzer, H., Warrener, A. G., and Hublin, J.-J. (2013). Trabecular evidence for a human-like gait in *Australopithecus africanus*. *PLoS One* 8:e77687. doi: 10.1371/journal.pone.0077687

Bayle, P., Bondioli, L., Macchiarelli, R., Mazurier, A., Puymerail, L., Volpato, V., et al. (2011). "Three-dimensional imaging and quantitative characterization of human fossil remains. Examples from the Nespos database," in *Pleistocene Databases: Acquisition Storing Sharing*, eds R. Macchiarelli, and G. C. Weniger (Mettmann: Wissenschaftliche Schriften des Neanderthal Museums 4), 29–46.

Bayle, P., Braga, J., Mazurier, A., and Macchiarelli, R. (2009). Dental developmental pattern of the Neanderthal child from Roc de Marsal: a high-resolution 3D analysis. *J. Hum. Evol.* 56, 66–75. doi: 10.1016/j.jhevol.2008.09.002

Beaudet, A. (2019). The inner ear of the *Paranthropus* specimen DNH 22 from Drimolen. *South Africa. Am. J. Phys. Anthropol.* 170, 439–446. doi: 10.1002/ajpa.23901

Beaudet, A., Braga, J., de Beer, F., Schillinger, B., Steininger, C., Vodopivec, V., et al. (2016). Neutron microtomography-based virtual extraction and analysis of a cercopithecoid partial cranium (STS 1039) embedded in a breccia fragment from Sterkfontein Member 4 (South Africa). *Am. J. Phys. Anthropol.* 159, 737–745. doi: 10.1002/ajpa.22916

Beaudet, A., Carlson, K. J., Clarke, R. J., de Beer, F., Dhaene, J., Heaton, J. L., et al. (2018). Cranial vault thickness variation and inner structural organization in the StW 578 hominin cranium from Jacovec Cavern. *South Africa. J. Hum. Evol.* 121, 204–220. doi: 10.1016/j.jhevol.2018.04.004

Beaudet, A., Zanolli, C., Engda Redae, B., Endalamaw, M., Braga, J., and Macchiarelli, R. (2015). A new cercopithecoid dentognathic specimen attributed to *Theropithecus* from the late Early Pleistocene (c. 1 Ma) deposits of Simbiro, at Melka Kunture. Ethiopian highlands. *C. R. Palevol.* 14, 657–669. doi: 10.1016/j.crpv.2015.07.003

Benazzi, S., Douka, K., Fornai, C., Bauer, C. C., Kullmer, O., Svoboda, J., et al. (2011a). Early dispersal of modern humans in Europe and implications for Neanderthal behaviour. *Nature* 479, 525–528. doi: 10.1038/nature10617

Benazzi, S., Viola, B., Kullmer, O., Fiorenza, L., Harvati, K., Paul, T., et al. (2011b). A reassessment of the Neanderthal teeth from Taddeo cave (southern Italy). *J. Hum. Evol.* 61, 377–387. doi: 10.1016/j.jhevol.2011.05.001

Braga, J. (2016). "Non-invasive imaging techniques," in *A Companion to Dental Anthropology*, eds J. D. Irish, and G. R. Scott (Chichester: John Wiley & Sons, Inc), 514–527.

Braga, J., Thackeray, F., Subsol, G., Kahn, J. L., Maret, D., Treil, J., et al. (2010). The enamel-dentine junction in the postcanine dentition of *Australopithecus africanus*: intra individual metameric and antimeric variation. *J. Anat.* 216, 62–79. doi: 10.1111/j.1469-7580.2009.01154.x

Cazenave, M., Braga, J., Oettlé, A., Pickering, T. R., Heaton, J. L., Nakatsukasa, M., et al. (2019a). Cortical bone distribution in the femoral neck of *Paranthropus robustus*. *J. Hum. Evol.* 135:102666. doi: 10.1016/j.jhevol.2019.102666

Cazenave, M., Oettlé, A., Thackeray, J. F., Nakatsukasa, M., de Beer, F., Hoffman, J., et al. (2019b). The SKX 1084 hominin patella from swartkrans member 2, South Africa: an integrated analysis of its outer morphology and inner structure. *C. R. Palevol.* 18, 223–235. doi: 10.1016/j.crpv.2018.06.002

Ciochon, R. (2009). The mystery ape of Pleistocene Asia. *Nature* 459, 910–911. doi: 10.1038/459910a

Conroy, G. C., and Vannier, M. W. (1985). "Endocranial volume determination of matrix-filled fossil skulls using high resolution computed tomography," in *Hominid Evolution: Past Present and Future*, ed. P. V. Tobias (New York, NY: Alan R. Liss, Inc), 419–426.

Conroy, G. C., and Vannier, M. W. (1987). Dental development of the Taung skull from computerized tomography. *Nature* 329, 625–627. doi: 10.1038/329625a0

Daegling, D. J. (1989). Biomechanics of cross-sectional size and shape in the hominoid mandibular corpus. *Am. J. Phys. Anthropol.* 80, 91–106. doi: 10.1002/ajpa.1330800111

Dehm, R. (1983). "Miocene hominoid primate dental remains from the Siwaliks of Pakistan," in *New Interpretations of Ape and Human Ancestry*, eds R. L. Ciochon, and R. S. Corruccini (New York, NY: Plenum Publishing Corporation), 527–537. doi: 10.1007/978-1-4684-8854-8_20

DeSilva, J. M., and Devlin, M. J. (2012). A comparative study of the trabecular bony architecture of the talus in humans, non-human primates, and Australopithecus. *J. Hum. Evol.* 63, 536–551. doi: 10.1016/j.jhevol.2012.06.006

Dubois, E. (1894). *Pithecanthropus erectus, Eine Menschenaehnliche Ubergangsform Aus Java*. Batavia: Landesdruckerei.

Elliott, J. C., and Dover, S. D. (1982). X-ray microtomography. *J. Microsc.* 126, 211–213.

Genochio, L., Mazurier, A., Dumoncel, J., Theye, C. E. G., and Zanolli, C. (2019). Inner structural organization of the mandibular corpus in the late Early Pleistocene human specimens Tighenif 1 and Tighenif 2. *C. R. Palevol.* 18, 1073–1082. doi: 10.1016/j.crpv.2019.09.002

Gorjanović-Kramberger, D. (1906). "Der diluviale mensch von krapina in kroatien: ein beitrag zur paläoanthropologie," in *Studien über die Entwicklungs-Mechanik des Primatenskeletes. Kreidel, Wiesbaden*, Vol. II, ed. O. Walkhoff (Wiesbaden: Kreidel), 59–277.

Gorjanović-Kramberger, D. (1907). Die kronen und wurzeln der mahlzähne des *Homo primigenius* und ihre genetische bedeutung. *Anat. Anz.* 31, 97–134.

Grine, F. E., Leakey, M. G., Gathago, P. N., Brown, F. H., Mongle, C. S., Yang, D., et al. (2019). Complete permanent mandibular dentition of early *Homo* from the upper burgi member of the koobi fora formation. *Ileret, Kenya. J. Hum. Evol.* 131, 152–175. doi: 10.1016/j.jhevol.2019.03.017

Guatelli-Steinberg, D. (2016). *What Teeth Reveal about Human Evolution*. Cambridge: Cambridge University Press.

Haile-Selassie, Y., Melillo, S. M., and Su, D. F. (2016). The Pliocene hominin diversity conundrum: do more fossils mean less clarity? *Proc. Nat. Acad. Sci. U.S.A.* 113, 6364–6371. doi: 10.1073/pnas.1521266113

Haile-Selassie, Y., Melillo, S. M., Vazzana, A., Benazzi, S., and Ryan, T. M. (2019). A 3.8-million-year-old hominin cranium from Woranso-Mille. *Ethiopia. Nature* 573, 214–219. doi: 10.1038/s41586-019-1513-8

Hillson, S. (2014). *Tooth Development in Human Evolution and Bioarchaeology*. Cambridge: Cambridge University Press.

Hounsfield, G. N. (1973). Computerized transverse axial scanning (tomography): i. description of system. *Brit. J. Radiol.* 46, 1016–1022. doi: 10.1259/0007-1285-46-552-1016

Hounsfield, G. N. (1975). *Method of and Apparatus for Examining a Body by Radiation such as X or Gamma Radiation*. Patent specification 1283915. Bangalore: The Patent Office.

Hublin, J.-J. (2013). Free digital scans of human fossils. *Nature* 497:183. doi: 10.1038/497183a

Immel, A., Le Cabec, A., Bonazzi, M., Herbig, A., Temming, H., Schuenemann, V. J., et al. (2016). Effect of X-ray irradiation on ancient DNA in sub-fossil bones – Guidelines for safe X-ray imaging. *Sci. Rep.* 6:32969. doi: 10.1038/srep32969

Jaeger, J.-J., Aung Naing Soe, A. N., Chavasseau, O., Coster, P., Emonet, E.-G., Guy, F., et al. (2011). First hominoid from the Late Miocene of the Irrawaddy Formation (Myanmar). *PLoS One* 6:e17065. doi: 10.1371/journal.pone.0017065

Jungers, W. L., and Minns, F. L. J. (1979). Computed tomography and biomechanical analysis of fossil long bones. *Am. J. Phys. Anthropol.* 50, 285–290. doi: 10.1002/ajpa.1330500219

Kaifu, Y., Baba, H., Aziz, F., Indriati, E., Schrenk, F., and Jacob, T. (2005). Taxonomic affinities and evolutionary history of the Early Pleistocene hominids of Java: dentognathic evidence. *Am. J. Phys. Anthropol.* 128, 709–726. doi: 10.1002/ajpa.10425

Kappelman, J., Ketcham, R. A., Pearce, S., Todd, L., Akins, W., Colbert, M. W., et al. (2016). Perimortem fractures in Lucy suggest mortality from fall out of tall tree. *Nature* 537, 503–507. doi: 10.1038/nature19332

Kardjilov, N., Baechler, S., Bastürk, M., Dierick, M., Jolie, J., Lehmann, E., et al. (2003). New features in cold neutron radiography and tomography. Part II: applied energy-selective neutron radiography and tomography. *Nucl. Instr. Meth. Phys. Res. A* 501, 536–546. doi: 10.1016/s0168-9002(03)00423-6

Keith, A. (1913). Problems relating to the teeth of the earlier forms of prehistorical man. *Proc. Roy. Soc. Med.* 6, 103–119.

Kelley, J. (1988). A new large species of *Sivapithecus* from the Siwaliks of Pakistan. *J. Hum. Evol.* 17, 305–324. doi: 10.1016/0047-2484(88)90073-5

Kelley, J. (2002). "The hominoid radiation in Asia," in *The Primate Fossil Record*, ed. W. Hartwig (Cambridge: Cambridge University Press), 369–384.

Kivell, T. L. (2016). A review of trabecular bone functional adaptation: what have we learned from trabecular analyses in extant hominoids and what can we apply to fossils? *J. Anat.* 228, 569–594. doi: 10.1111/joa.12446

Kullmer, O. (2008). The fossil suidae from the Plio-Pleistocene Chiwondo beds of northern Malawi, Africa. *J. Vert. Paleont.* 208, 208–216. doi: 10.1671/0272-4634(2008)28[208:TFSFTP]2.0.CO;2

Kullmer, O., Sandrock, O., Kupczik, K., Frost, S. R., Volpato, V., Bromage, T. G., et al. (2011). New primate remains from Mwenirondo, Chiwondo beds in northern Malawi. *J. Hum. Evol.* 61, 617–623. doi: 10.1016/j.jhevol.2011.07.003

Kupczik, K., Delezene, L. K., and Skinner, M. M. (2019). Mandibular molar root and pulp cavity morphology in *Homo naledi* and other Plio-Pleistocene hominins. *J. Hum. Evol.* 130, 83–95. doi: 10.1016/j.jhevol.2019.03.007

Kupczik, K., and Hublin, J.-J. (2010). Mandibular molar root morphology in Neanderthals and Late Pleistocene and recent *Homo sapiens*. *J. Hum. Evol.* 59, 525–541. doi: 10.1016/j.jhevol.2010.05.009

Lakey, J. H. (2009). Neutrons for biologists: a beginner's guide, or why you should consider using neutrons. *J. R. Soc. Interface* 6, S567–S573. doi: 10.1098/rsif.2009.0156.focus

Le Cabec, A., Dean, M. C., and Begun, D. (2017). Dental development and age at death of the holotype of *Anapithecus hernyaki* (RUD 9) using synchrotron virtual histology. *J. Hum. Evol.* 108, 161–175. doi: 10.1016/j.jhevol.2017.03.007

Le Cabec, A., Gunz, P., Kupczik, K., Braga, J., and Hublin, J.-J. (2013). Anterior tooth root morphology and size in Neanderthals: taxonomic and functional implications. *J. Hum. Evol.* 64, 169–193. doi: 10.1016/j.jhevol.2012.08.011

Le Cabec, A., Tang, N., and Tafforeau, P. (2015). Accessing developmental information of fossil hominin teeth using new synchrotron microtomography-based visualization techniques of dental surfaces and interfaces. *PLoS One* 10:e0123019. doi: 10.1371/journal.pone.0123019

Le Cabec, A., and Toussaint, M. (2017). Impacts of curatorial and research practices on the preservation of fossil hominid remains. *J. Anthropol. Sci.* 95, 7–34. doi: 10.4436/JASS.95002

Le Roux, S. D., de Beer, F., and Thackeray, J. F. (1997). Neutron radiography of cranial bone of Sts 5 (*Australopithecus africanus*) from Sterkfontein. *South Afr.. S. Afr. J. Sci.* 93:176.

Lehmann, E. H. (2017). Neutron imaging facilities in a global context. *J. Imaging* 3, 52. doi: 10.3390/jimaging3040052

Lüdecke, T., Kullmer, O., Wacker, U., Sandrock, O., Fiebig, J., Schrenk, F., et al. (2018). Dietary versatility of Early Pleistocene hominins. *Proc. Nat. Acad. Sci. U.S.A.* 115, 13330–13335. doi: 10.1073/pnas.1809439115

Macchiarelli, R., Bayle, P., Bondioli, L., Mazurier, A., and Zanolli, C. (2013). "From outer to inner structural morphology in dental anthropology. The integration of the third dimension in the visualization and quantitative analysis of fossil remains," in *Anthropological Perspectives on Tooth Morphology: Genetics, Evolution, Variation*, eds R. G. Scott, and J. D. Irish (Cambridge: Cambridge University Press), 250–277. doi: 10.1017/cbo9780511984464.011

Macchiarelli, R., Bondioli, L., Debénath, A., Mazurier, A., Tournepiche, J.-F., Birch, W., et al. (2006). How Neanderthal molar teeth grew. *Nature* 444, 748–751. doi: 10.1038/nature05314

Macchiarelli, R., Bondioli, L., Falk, D., Faupl, P., Illerhaus, B., Kullmer, O., et al. (2004). Early Pliocene hominid tooth from Galili, Somali Region, Ethiopia. *Coll. Antropol.* 28, 65–76.

Macchiarelli, R., Bondioli, L., and Mazurier, A. (2008). "Virtual dentitions: touching the hidden evidence," in *Technique and Application in Dental Anthropology*, eds J. D. Irish, and G. C. Nelson (Cambridge: Cambridge University Press), 426–448. doi: 10.1017/cbo9780511542442.018

Macchiarelli, R., Mazurier, A., Illerhaus, B., and Zanolli, C. (2009). *Ouranopithecus macedoniensis* (Mammalia, Primates, Hominoidea): virtual reconstruction and 3D analysis of a juvenile mandibular dentition (RPl-82 and RPl-83). *Geodiversitas* 31, 851–864.

Macchiarelli, R., Mazurier, A., and Volpato, V. (2007). "L'apport des nouvelles technologies à l'étude des Néandertaliens," in *Les Néandertaliens. Biologie et Cultures*, eds B. Vandermeersch, and B. Maureille (Paris: : Comité des Travaux Historiques et Scientifiques), 169–179.

Macchiarelli, R., and Weniger, G.-C. (eds) (2011). *Pleistocene Databases. Acquisition, Storing, Sharing*. Mettmann: Wissenschaftliche Schriften des Neanderthal Museums 4.

Macchiarelli, R., and Zanolli, C. (2017). Hominin Biomechanics, virtual anatomy and inner structural morphology: from head to toe. A tribute to laurent puymerail. *C. R. Palevol.* 16, 493–498. doi: 10.1016/j.crpv.2017.06.001

Maret, D., Ove, A. P., Galibourg, A., Dumoncel, J., Esclassan, R., Kahn, J. L., et al. (2014). Comparison of the accuracy of 3-dimensional cone-beam computed tomography and micro-computed tomography reconstructions by using different voxel sizes. *J. Endod.* 40, 1321–1326. doi: 10.1016/j.joen.2014.04.014

Martínez de Pinillos, M., Martinón-Torres, M., Martín-Francés, L., Arsuaga, J. L., and Bermúdez de Castro, J. M. (2017). Comparative analysis of the trigonid crests patterns in *Homo antecessor* molars at the enamel and dentine surfaces. *Quat. Int.* 433, 189–198. doi: 10.1016/j.quaint.2015.08.050

Martín-Francés, L., Martinón-Torres, M., Martínez de Pinillos, M., García-Campos, C., Modesto-Mata, M., Zanolli, C., et al. (2018). Tooth crown tissue proportions and enamel thickness in Early Pleistocene *Homo antecessor* molars (Atapuerca. Spain). *PLoS One* 13:e0203334. doi: 10.1371/journal.pone.0203334

Martinón-Torres, M., Bermúdez de Castro, J. M., Martínez de Pinillos, M., Modesto-Mata, M., Xing, S., Martín-Francés, L., et al. (2019). New permanent teeth from gran dolina-TD6 (Sierra de Atapuerca). The bearing of *Homo antecessor* on the evolutionary scenario of Early and Middle Pleistocene Europe. *J. Hum. Evol.* 127, 93–117. doi: 10.1016/j.jhevol.2018.12.001

Mazurier, A., Volpato, V., and Macchiarelli, R. (2006). Improved noninvasive microstructural analysis of fossil tissues by means of SR-microtomography. *Appl. Phys. A* 83, 229–233. doi: 10.1007/s00339-006-3511-6

Meschan, I., Bo, W. J., and Krueger, W. A. (1979). The utilization of xeroradiography for radiography of cross-section of thin cadaveric slices. *Invest. Radiol.* 14, 97–102. doi: 10.1097/00004424-197901000-00015

Olejniczak, A. J., and Grine, F. E. (2005). High-resolution measurement of Neanderthal tooth enamel thickness by micro-focal computed tomography. *South Afr. J. Sci.* 101, 219–220.

Olejniczak, A. J., and Grine, F. E. (2006). Assessment of the accuracy of dental enamel thickness measurements using microfocal X-ray computed tomography. *Anat. Rec.* 288, 263–275. doi: 10.1002/ar.a.20307

Olejniczak, A. J., Smith, T. M., Feeney, R. N. M., Macchiarelli, R., Mazurier, A., Bondioli, L., et al. (2008). Dental tissue proportions and enamel thickness in Neandertal and modern human molars. *J. Hum. Evol.* 55, 12–23. doi: 10.1016/j.jhevol.2007.11.004

Paganin, D. M., and Pellicia, D. (2019). Tutorials on X-ray phase contrast imaging: some fundamentals and some conjectures on future developments. *arXiv*. [preprint]. Avaliable at: https://arxiv.org/abs/1902.00364 (accessed January 29, 2020).

Pan, L., Thackeray, J. F., Dumoncel, J., Zanolli, C., Oettlé, A., de Beer, F., et al. (2017). Intra-individual metameric variation expressed at the enamel-dentine junction of lower post-canine dentition of South African fossil hominins and modern humans. *Am. J. Phys. Anthropol.* 163, 806–815. doi: 10.1002/ajpa.23240

Pan, L., and Zanolli, C. (2019). Comparative observations on the premolar root and pulp canal configurations of Middle Pleistocene *Homo* in China. *Am. J. Phys. Anthropol.* 168, 637–646. doi: 10.1002/ajpa.23777

Pilbeam, D. R. (1982). New hominoid skull material from the Miocene of Pakistan. *Nature* 295, 232–234. doi: 10.1038/295232a0

Puymerail, L., Ruff, C. B., Bondioli, L., Widianto, H., Trinkaus, E., and Macchiarelli, R. (2012a). Structural analysis of the Kresna 11 *Homo erectus* femoral shaft (Sangiran. Java). *J. Hum. Evol.* 63, 741–749. doi: 10.1016/j.jhevol.2012.08.003

Puymerail, L., Volpato, V., Debenath, A., Mazurier, A., Tournepiche, J.-F., and Macchiarelli, R. (2012b). A Neanderthal partial femoral diaphysis from the "grotte de la Tour", La Chaise-de-Vouthon (Charente, France): outer

morphology and endostructural organization. *C. R. Palevol.* 11, 581–593. doi: 10.1016/j.crpv.2012.07.001

Röntgen, W. (1895). "Ueber eine neue art von strahlen. *vorläufige mitteilung*," in *Aus den Sitzungsberichten der Würzburger Physik.-medic. Gesellschaft Würzburg* (Berlin: Springer-Verlag), 137–147.

Rook, L., Bondioli, L., Casali, F., Rossi, M., Köhler, M., Moyá Solá, S., et al. (2004). The bony labyrinth of *Oreopithecus bambolii*. *J. Hum. Evol.* 46, 345–352.

Rossi, M., Casali, F., Romani, D., Bondioli, L., Macchiarelli, R., and Rook, L. (2004). MicroCT scan in paleobiology: application to the study of dental tissues. *Nucl. Instr. Meth. Phys. Res. B* 213, 747–750. doi: 10.1016/s0168-583x(03)01697-5

Ruff, C. B., and Leo, F. P. (1986). Use of computed tomography in skeletal structure research. *Yearb. Phys. Anthropol.* 29, 181–196. doi: 10.1002/ajpa.1330290508

Ryan, T. M., Carlson, K. J., Gordon, A. D., Jablonski, N., Shaw, C. N., and Stock, J. T. (2018). Human-like hip joint loading in *Australopithecus africanus* and Paranthropus robustus. *J. Hum. Evol.* 121, 12–24. doi: 10.1016/j.jhevol.2018.03.008

Schillinger, B., Beaudet, A., Fedrigo, A., Grazzi, F., Kullmer, O., Laaβ, M., et al. (2018). Neutron imaging in cultural heritage research at the FRM II Reactor of the Heinz Maier-Leibnitz Center. *J. Imaging* 4:22. doi: 10.3390/jimaging4010022

Schoetensack, O. (1908). *Der Unterkiefer des Homo heidelbergensis aus den Sanden von Mauer bei Heidelberg*. Leipzig: Engelmann.

Schrenk, F., Bromage, T. G., Betzler, C. G., Ring, U., and Juwayeyi, Y. M. (1993). Oldest *Homo* and Pliocene biogeography of the malawi rift. *Nature* 365, 833–836. doi: 10.1038/365833a0

Schwarz, D., Vontobel, P., Lehmann, E. H., Meyer, C. A., and Bongartz, G. (2005). Neutron tomography of internal structures of vertebrate remains: a comparison with X-ray computed tomography. *Palaeontol. Electronica* 8:30A.

Scott, G. R., Turner, C. G. II, Townsend, G. C., and Martinón-Torres, M. (eds) (2018). *The Anthropology of Modern Human Teeth*. Cambridge: Cambridge University Press.

Skinner, M. F., and Sperber, G. H. (1982). *Atlas of Radiographs of Early Man*. New York, NY: A.R. Liss.

Skinner, M. M., Alemseged, Z., Gaunitz, C., and Hublin, J.-J. (2015). Enamel thickness trends in Plio-Pleistocene hominin mandibular molars. *J. Hum. Evol.* 85, 35–45. doi: 10.1016/j.jhevol.2015.03.012

Skinner, M. M., de Vries, D., Gunz, P., Kupczik, K., Klassen, R. P., Hublin, J.-J., et al. (2016). A dental perspective on the taxonomic affinity of the Balanica mandible (BH-1). *J. Hum. Evol.* 93, 63–81. doi: 10.1016/j.jhevol.2016.01.010

Skinner, M. M., Gunz, P., Wood, B. A., and Hublin, J.-J. (2008). Enamel-dentine junction (EDJ) morphology distinguishes the lower molars of *Australopithecus africanus* and *Paranthropus robustus*. *J. Hum. Evol.* 55, 979–988. doi: 10.1016/j.jhevol.2008.08.013

Skinner, M. M., Kivell, T. L., Potze, S., and Hublin, J.-J. (2013). Microtomographic archive of fossil hominin specimens from Kromdraai B. *South Afr. J. Hum. Evol.* 64, 434–447. doi: 10.1016/j.jhevol.2013.01.007

Smilg, J. S., and Berger, L. R. (2015). Discovering hominins - application of medical computed tomography (CT) to fossil-bearing rocks from the site of Malapa. South Africa. *PLoS One* 10:e0145340. doi: 10.1371/journal.pone.0145340

Smith, T. M., Houssaye, A., Kullmer, O., Le Cabec, A., Olejniczak, A. J., Schrenk, F., et al. (2018). Disentangling isolated dental remains of Asian Pleistocene hominins and pongines. *PLoS One* 13:e0204737. doi: 10.1371/journal.pone.0204737

Smith, T. M., Olejniczak, A. J., Kupczik, K., Lazzari, V., de Vos, J. C., Kullmer, O., et al. (2009). Taxonomic assessment of the Trinil molars using non-destructive 3D structural and development analysis. *Paleo Anthropol.* 2009, 117–129.

Smith, T. M., and Tafforeau, P. (2008). New visions of dental tissue research: tooth development, chemistry, and structure. *Evol. Anthropol.* 17, 213–226. doi: 10.1002/evan.20176

Smith, T. M., Tafforeau, P., Le Cabec, A., Bonnin, A., Houssaye, A., Pouech, J., et al. (2015). Dental ontogeny in Pliocene and Early Pleistocene hominins. *PLoS One* 10:e0118118. doi: 10.1371/journal.pone.0118118

Spoor, F., Gunz, P., Neubauer, S., Stelzer, S., Scott, N., Kwekason, A., et al. (2015). Reconstructed *Homo habilis* type OH 7 suggests deep-rooted species diversity in early Homo. *Nature* 519, 83–86. doi: 10.1038/nature14224

Spoor, F., Jeffery, N., and Zonneveld, F. (2000). "Imaging skeletal growth and evolution," in *Development, Growth and Evolution: Implications for the Study of the Hominid Skeleton*, eds P. O'Higgins, and M. Cohn (San Diego: Academic Press for the Linnean Society of London), 123–161.

Spoor, F., Wood, B., and Zonneveld, F. (1994). Implications of early hominid labyrinthine morphology for evolution of human bipedal locomotion. *Nature* 369, 645–648. doi: 10.1038/369645a0

Sutton, M. D. (2008). Tomographic techniques for the study of exceptionally preserved fossils. *Proc. R. Soc. B* 275, 1587–1593. doi: 10.1098/rspb.2008.0263

Tafforeau, P., Boistel, R., Boller, E., Bravin, A., Brunet, M., Chaimanee, Y., et al. (2006). Applications of X-ray synchrotron microtomography for non-destructive 3D studies of paleontological specimens. *Appl. Phys. A* 83, 195–202. doi: 10.1073/pnas.0807047106

Tafforeau, P., and Smith, T. M. (2008). Nondestructive imaging of hominoid dental microstructure using phase contrast X-ray synchrotron microtomography. *J. Hum. Evol.* 54, 272–278. doi: 10.1016/j.jhevol.2007.09.018

Tafforeau, P., Zermeno, J. P., and Smith, T. M. (2012). Tracking cellular-level enamel growth and structure in 4D with synchrotron imaging. *J. Hum. Evol.* 62, 424–428. doi: 10.1016/j.jhevol.2012.01.001

Tate, J. R., and Cann, C. E. (1982). High-resolution computed tomography for the comparative study of fossil and extant bone. *Am. J. Phys. Anthropol.* 58, 67–73. doi: 10.1002/ajpa.1330580108

Tremsin, A. S., McPhate, J. B., Vallerga, J. V., Siegmund, O. H. W., Feller, W. B., Lehman, E., et al. (2011). High-resolution neutron microtomography with noiseless neutron counting detector. *Nucl. Instr. Meth. Phys. Res. A* 652, 400–403. doi: 10.1016/j.nima.2010.08.009

Tremsin, A. S., Morgano, M., Panzner, T., Lehmann, E., Filgers, U., Vallerga, J. V., et al. (2015). High resolution neutron imaging capabilities at BOA beamline at Paul Scherrer Institut. *Nucl. Instr. Meth. Phys. Res. A* 784, 486–493. doi: 10.1016/j.nima.2014.09.026

Trinkaus, E. (1984). "Western Asia," in *in The Origins of Modern Humans: A World Survey of the Fossil Evidence*, eds F. H. Smith, and F. Spencer (New York, NY: Alan R. Liss, Inc), 251–293.

Tyler, D. E. (2004). An examination of the taxonomic status of the fragmentary mandible Sangiran 5, (*Pithecanthropus dubius*). *Homo erectus*, "*Meganthropus*", or *Pongo*? *Quat. Int.* 117, 125–130. doi: 10.1016/s1040-6182(03)00122-8

Ulhaas, L. (2007). "Computer-based reconstruction: technical aspects and application," in *Handbook of Palaeoanthopology*, eds W. Henke, and I. Tattersall (Berlin: Springer), 787–814.

Urciuoli, A., Zanolli, C., Fortun, J., Almécija, S., Schillinger, B., Moyà-Solà, S., et al. (2017). Neutron-based computed microtomography: *Pliobates cataloniae* and *Barberapithecus huerzeleri* as a test-case study. *Am. J. Phys. Anthropol.* 166, 987–993. doi: 10.1002/ajpa.23467

Villmoare, B. (2018). Early *Homo* and the role of the genus in palaeoanthropology. *Am. J. Phys. Anthropol.* 165, 72–89. doi: 10.1002/ajpa.23387

von Koenigswald, G. H. R. (1950). Fossil hominids of the lower Pleistocene of Java. 18th Intl. *Geol. Congr.* 9, 59–61.

Walkhof, O. (1902). *Der Unterkiefer der Anthropomorphen und des Menschen in Seiner Funktionellen Entwickelung und Gestalt*. Wiesbaden: C. W. Kreidel's Verlag.

Ward, S. C., and Brown, B. (1986). "The facial skeleton of *Sivapithecus indicus*," in *Comparative Primate Biology Systematics, Evolution and Anatomy*, Vol. 1, Chap. New York, NY, eds D. Swindler, and S. Erwin (Alan R. Liss), 413–452.

Weber, G. W., and Bookstein, F. L. (2011). *Virtual Anthropology. A Guide to a New Interdisciplinary Field*. Wien: Springer.

Weidenreich, F. (1945). Giant early man from Java and South China. *Anthropol. Pap. Am. Mus. Nat. Hist.* 40, 1–134.

Wind, J. (1984). Computerized x−ray tomography of fossil hominid skulls. *Am. J. Phys. Anthropol.* 63, 265–282. doi: 10.1002/ajpa.1330630303

Wind, J., and Zonneveld, F. W. (1989). Computed tomography of an *Australopithecus* skull (Mrs Ples): a new technique. *Naturwissenschaften* 76, 325–327. doi: 10.1007/bf00368433

Winkler, B. (2006). Applications of neutron radiography and neutron tomography. *Rev. Min. Geochem.* 63, 459–471. doi: 10.2138/rmg.2006.63.17

Wood, B. (2011). *Wiley-Blackwell Encyclopedia of Human Evolution*. Chichester: Blackwell Publishing Ltd.

Wood, B. A., and Boyle, E. K. (2016). Hominin taxic diversity: Fact or fantasy? *Yearb. Phys. Anthropol.* 159, S37–S78. doi: 10.1002/ajpa.22902

Wu, X., and Schepartz, L. A. (2009). Application of computed tomography in paleoanthropological research. *Progr. Nat. Sci.* 19, 913–921. doi: 10.1016/j.pnsc.2008.10.009

Xing, S., Tafforeau, P., O'Hara, M., Modesto-Mata, M., Martín-Francés, L., Martinón-Torres, M., et al. (2019). First systematic assessment of dental growth and development in an archaic hominin (genus, *Homo*) from East Asia. *Sci. Advances* 5:eaau0930. doi: 10.1126/sciadv.aau0930

Zanolli, C. (2015). Molar crown inner structural organization in Javanese *Homo erectus*. *Am. J. Phys. Anthropol.* 156, 148–157. doi: 10.1002/ajpa.22611

Zanolli, C., Bondioli, L., Coppa, A., Dean, M. C., Bayle, P., Candilio, F., et al. (2014). The late Early Pleistocene human dental remains from Uadi Aalad and Mulhuli-Amo (Buia), Eritrean Danakil: macromorphology and microstructure. *J. Hum. Evol.* 74, 96–113. doi: 10.1016/j.jhevol.2014.04.005

Zanolli, C., Bondioli, L., Mancini, L., Mazurier, A., Widianto, H., and Macchiarelli, R. (2012). Two human fossil deciduous molars from the Sangiran Dome (Java, Indonesia): outer and inner morphology. *Am. J. Phys. Anthropol.* 147, 472–481. doi: 10.1002/ajpa.21657

Zanolli, C., Dean, M. C., Assefa, Y., Bayle, P., Braga, J., Condemi, S., et al. (2017a). Structural organization and tooth development in a *Homo* aff. *erectus* juvenile mandible from the Early Pleistocene site of Garba IV at Melka Kunture, Ethiopian highlands. *Am. J. Phys. Anthropol.* 162, 533–549. doi: 10.1002/ajpa.23135

Zanolli, C., Grine, F. E., Kullmer, O., Schrenk, F., and Macchiarelli, R. (2015). The Early Pleistocene deciduous hominid molar FS-72 from the Sangiran Dome of Java, Indonesia: a taxonomic reappraisal based on its comparative endostructural characterization. *Am. J. Phys. Anthropol.* 157, 666–674. doi: 10.1002/ajpa.22748

Zanolli, C., Kullmer, O., Kelley, J., Bacon, A.-M., Demeter, F., Dumoncel, J., et al. (2019a). Evidence for increased hominid diversity in the Early-Middle Pleistocene of Indonesia. *Nature Ecol. Evol.* 3, 755–764. doi: 10.1038/s41559-019-0860-z

Zanolli, C., Martinón-Torres, M., Bernardini, F., Boschian, G., Coppa, A., Dreossi, D., et al. (2018a). The Middle Pleistocene (MIS 12) human dental remains from Fontana Ranuccio (Latium) and Visogliano (Friuli-Venezia Giulia), Italy. A comparative high resolution endostructural assessment. *PLoS One* 13:e0189773. doi: 10.1371/journal.pone.0189773

Zanolli, C., and Mazurier, A. (2013). Endostructural characterization of the *H. heidelbergensis* dental remains from the early Middle Pleistocene site of Tighenif, Algeria. *C. R. Palevol.* 12:293–304. doi: 10.1016/j.crpv.2013.06.004

Zanolli, C., Pan, L., Dumoncel, J., Kullmer, O., Kundrát, M., Liu, W., et al. (2018b). Inner tooth morphology of *Homo erectus* from Zhoukoudian. New evidence from an old collection housed at Uppsala University, Sweden. *J. Hum. Evol.* 116, 1–13. doi: 10.1016/j.jhevol.2017.11.002

Zanolli, C., Schillinger, B., Beaudet, A., Kullmer, O., Macchiarelli, R., Mancini, L., et al. (2017b). Exploring hominin and non-hominin primate dental fossil remains with neutron microtomography. *Phys. Procedia* 88, 109–115. doi: 10.1016/j.phpro.2017.06.014

Zanolli, C., Skinner, M. M., Schrenk, F., Bromage, T. G., Hublin, J.-J., Schillinger, B., et al. (2019b). Taxonomic revision of the initial Early Pleistocene HCRP-U18-501 hominin mandible from Malawi: a tooth internal structural perspective. *Proc. Eur. Soc. Hum. Evol.* 8:206.

Zollikofer, C. P. E., and Ponce de León, M. S. (2005). *Virtual Reconstruction: A Primer in Computer-Assisted Paleontology and Biomedicine*. Hoboken: J. Wiley & Sons, Inc.

Zonneveld, F. W., and Wind, J. (1985). "High resolution computed tomography of fossil hominid skulls: a new method and some results," in *Hominid Evolution: Past, Present and Future*, ed. P. V. Tobias (New York, NY: Alan R. Liss, Inc), 427–436.

Conflict of Interest: The authors declare that the research was conducted in the absence of any commercial or financial relationships that could be construed as a potential conflict of interest.

Copyright © 2020 Zanolli, Schillinger, Kullmer, Schrenk, Kelley, Rössner and Macchiarelli. This is an open-access article distributed under the terms of the Creative Commons Attribution License (CC BY). The use, distribution or reproduction in other forums is permitted, provided the original author(s) and the copyright owner(s) are credited and that the original publication in this journal is cited, in accordance with accepted academic practice. No use, distribution or reproduction is permitted which does not comply with these terms.